Control of Turbulent Transport by GAMs

K. Hallatschek, R. Hager

Max-Planck-Institut für Plasmaphysik, EURATOM Association, D-85748 Garching, Germany

E-mail: Klaus.Hallatschek@ipp.mpg.de

Abstract. In the tokamak edge, quasi-stationary zonal flows are strongly suppressed, and the turbulence saturation is effected by several concurrent mechanisms including geodesic acoustic modes (GAMs). GAMs could offer a tempting way to control the turbulence independent of the properties of the turbulence modes themselves. However, at present they have been experimentally observed only at rather weak displacement amplitudes compared to circular turbulence computations. It has been explored by numerical turbulence studies in how far flux surface ellipticity and the very high gradients encountered in the edge affect the GAM intensity. Since experimental flux surfaces have subtle interdependences between the various geometrical parameters, they are not well suitable to discriminate effects on the GAM from the ones on the turbulence. Therefore, a geometry variation has been chosen which maintains the turbulence properties (growth rate, structure) at the outboard midplane as constant as possible, while varying the linear GAM properties through the global properties of the flux surfaces. That way, for the variation of ellipticity a strong saturating effect mediated via the GAMs can be shown quite convincingly. In the absence of diamagnetic effects, such as for pure resistive ballooning turbulence, the diamagnetic GAM drive is switched off and the GAMs are suppressed. However for sufficiently high gradients, the GAMs return because the ratio of turbulence free energy stored in the pressure fluctuations to the turbulence kinetic energy rises, whereas the GAMs themselve maintain equal fractions of fluctuation and kinetic energy. This results in a relative rise of the GAM kinetic energy in comparison to the turbulent kinetic energy, which significantly reduces the turbulence to intensities well below the mixing length estimate. In the limit of infinite gradients, a quasistationary flow pattern results, which completely suppresses the transport. Moreover, in the edge regime relevant to the GAMs, the plasma parameters change so rapidly that radial drifts conveyed by the group velocity of the GAMs can become important. It is shown that the turbulence itself can be responsible for the dominant part of that effect.

1. Introduction

While at present there is a tendency to ascribe the saturation of all forms of tokamak turbulence to quasi-stationary zonal flows (ZF), this is not the case in edge turbulence, where the ZFs are strongly suppressed due to the long connection length there [1]. In the edge there are several concurrent saturation mechanisms whereby saturation by geodesic acoustic modes (GAM), oscillating global flows, has some similarities to the one by core ZF and is the only one experimentally detectable and susceptible to plasma parameters and geometry, independent of the turbulence. Although GAMs potentially offer a way to control the local turbulence, experimental measurements of their amplitude so far seem to be limited to cases of rather weak activity with displacement amplitudes of $\lesssim$ 1cm [5, 6], which are unlikely to seriously reduce the turbulence amplitudes as effectively as seen in turbulence simulations for the transitional regime in [4].

One difference is the simplistic circular geometry used in those simulations, whence it has been explored in how far flux surface ellipticity modifies GAM activity and its impact on the turbulence. Studying moreover the effect of the (experimentally uncertain) background gradients on the GAM activity, it was found that very high gradients in particular can cause rather strong GAMs with a substantial impact on the transport.
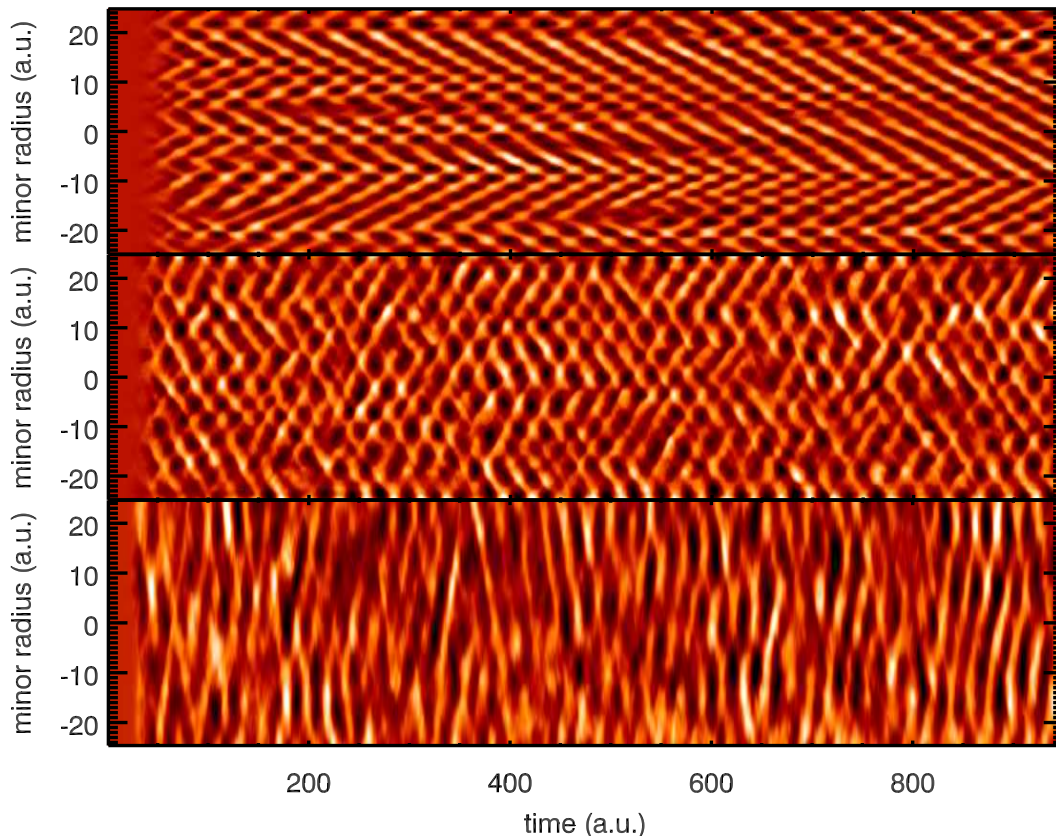
Figure 1: Color coded GAM poloidal flow velocity for $\kappa = 1.7$ (top), $\kappa = 1$ (middle), $\kappa = 0.5$; note the different scale lengths and frequencies.

Moreover, the rapid change of the parameters – in particular that of the sound speed being proportional to the linear GAM frequency – renders the radial interaction of the GAMs on neighbouring flux surface [9, 10] quite important, and raises the question in what spatial pattern the GAMs will organize themselves. This could involve reflection layers exhibiting a peaking of the GAMs, radial propagation of GAM energy away from turbulent regions generating it, or nonlinear changes of the GAM dispersion relation.

Numerical turbulence studies were performed with the NLET code [7] using two-fluid electrostatic Braginskii equations with modified parallel heat conduction coefficient implementing a collisionless heat flux limit. The magnetic geometry was represented by local Miller-equilibria [8].

2. Ellipticity

When simply using the experimental flux surface shape in turbulence simulations it is quite hard to separate the geometry effect on the turbulence itself from the one on the GAMs, while on the other hand experimentally neither the magnetic geometry nor the gradients in the plasma are sufficiently accurately known to determine the correct turbulence regime. Changing the magnetic geometry of computer turbulence studies in a straightforward manner thus usually results in qualitatively different types of turbulence for the different geometries, which cannot be compared with each other. Empirically it turns out that fixing the ratio of gradient lengths, magnetic curvature radii and the local shear length at the outboard midplane results in well comparable scenarios.
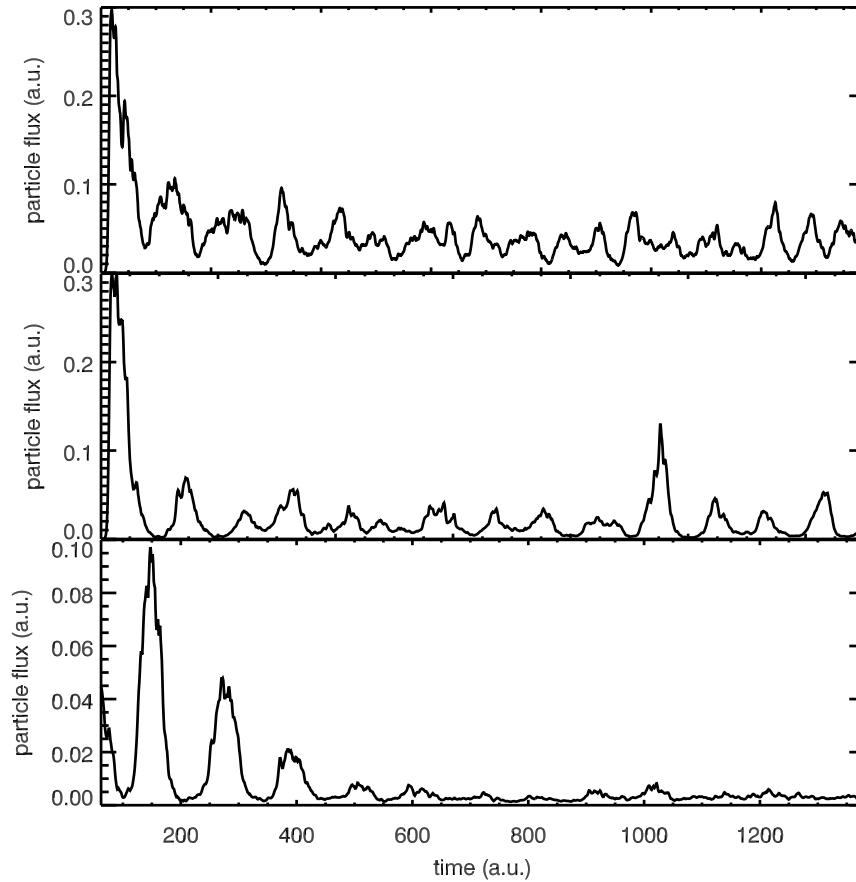
Figure 2: Time evolution of particle flux for isothermal resistive ballooning turbulence simulation with $L_p/R = 0.01$ (top), 0.0025 (middle), 0 (bottom) in the respective mixing length units. Particle flux becomes bursty and eventually dies out in the limit of large gradients.

Fig. 1 compares GAM flow-patterns for ellipticity $\kappa = 0.5, 1, 1.7$ and concomittant $s_\kappa \equiv d\ln\kappa/d\ln r = -0.5, 0, 0.7$, respectively, with ratio of connection length to local shear length at the outboard midplane $L_c/L_s = 2\pi$ corresponding to total shear $s = 1$ for circular concentric flux surfaces. The total shear $d\ln q/d\ln r$ (r is the Miller radius) was $0.47, 1.00, 2.95$, respectively. The other parameters were taken to be identical as in [4]. Apart from the change in frequency, which follows the linear predictions, the flow patterns are qualitatively identical. The turbulent heat fluxes were, respectively, $\chi(\rho_s^2 c_s/R) = 10, 1.0, 0.10$, while the RMS flow levels are $\langle|v_\theta|\rangle/v_{di,e} = 0.95, 1.64, 1.44$. To clarify, whether the tenfold transport reduction for each step of increasing ellipticity is in part due to the GAMs, the turbulence simulations for $\kappa = 1$ and 1.7 have been restarted, while artificially suppressing the flux surface averaged poloidal flows. This yielded the transport coefficients $\chi(\rho_s^2 c_s/R) = 10, 2.5$, which are an order of magnitude larger and also show less favourable influence from the ellipticity than the runs with self-consistent GAMs.

2. High gradient regime

In the absence of diamagnetic velocities, such as for pure resistive ballooning turbulence, the diamagnetic drive [1] is completely switched off, whence for normal edge gradients GAM activity is suppressed [4]. However, for sufficiently high gradients, the GAMs return. Fig. 2 shows the space-average particle flux for isothermal resistive ballooning turbulence at varying

gradients in mixing length units as a function of time. The flux shows a marked decrease and a transition from continuous transport to bursts due to the GAM oscillations, while it would be constant due to the mixing length normalisation if the turbulence were saturating by a turbulent cascade.

The reason for this change is the behavior of the ratio of turbulence kinetic energy E_ϕ to fluctuation free energy E_p. It can be estimated order-of-magnitudewise in the mixing-length framework as follows: During an eddy turn over time – one step in a random walk process for the pressure fluctuations – a percentage $\propto L_p/R$ (L_p is the pressure gradient length, R the curvature,i.e. major, radius) of the fluctuation free energy is converted into kinetic energy by expansion of the plasma in the inhomogeneous magnetic field, while the rest is dissipated. Therefore,

$$\frac{E_\phi}{E_p} \sim \frac{v^2}{\delta p^2} \propto \frac{L_p}{R} \ll 1$$

where δp and v are the typical pressure and velocity fluctuation amplitudes. For sufficiently large gradients $L_p \ll R$ and $v^2 \ll \delta p^2$, whence the Reynolds stress is negligible compared to the GAM drive by asymmetric anomalous transport [4] via the Stringer-Winsor force (SW). Since the average GAM amplitude is then in balance with the SW drive (and not the Reynolds stress), it is scaled up in comparison to the turbulence velocities for increasing gradients, eventually suppressing the turbulence.

In the limit $L_p/R \to 0$ a quasistationary flow pattern results, which completely suppresses the transport (in mixing length units).

3. Radial propagation at rapidly varying parameters

The rate of parameter variation can be described by the local ratio of turbulence to background gradient scale lengths $\lambda^{-1} = L_\perp/L_n \propto \rho^* = \rho_s/R$, with the turbulence scale length $L_\perp$, whereby $\lambda \sim 5-50$ for typical edge scenarios.

Fig. 3 shows GAMs being excited by high gradient ITG modes in a case of still moderate parameter variation, $\lambda = 200$. From the flow pattern (a) it is obvious that the oscillation frequency decreases towards the edge, which is due to the decreasing sound speed, otherwise apparently rather unaffected by the parameter variation. As is seen in Boussinesq simulations [4], the GAMs are excited with a preferred radial wavenumber, which together with the linear GAM frequency sets the observed inward and outward phase velocities. The Fourier transform of the poloidal flow velocity with respect to time (b) reveals that the frequency depends continuously on the spatial variable. An asymmetry is however conspicuous in the spectrum: there is an amplitude of the GAMs of a particular frequency even at somewhat larger radii than the one corresponding to their linear frequency (blue line), but not the other way round. The GAMs *radiate outward* from a given radius. The cause for this effect can be gleaned by transforming selectively one frequency of the Fourier representation into real space, as shown in (c). The particular GAM is seen to correspond to a wave travelling inward (to lower radii) and being reflected by the surface corresponding to $k_r = 0$. This can be comfirmed by comparison of the shape of the waves close to the reflection with the one obtained from a generic GAM dispersion relation. We approximate the GAM dispersion relation close to $k_r = 0$ by

$$\omega_{GAM}(r,k_r) = \omega_{GAM}(r,0)(1+\alpha k_r^2) = \gamma c_s(r)(1+\alpha k_r^2), \tag{1}$$

where γ is the geometry dependent ratio of GAM frequency and sound speed and α sets the strength of the dispersion (the linear term has to vanish for symmetry reasons). (As it turns out
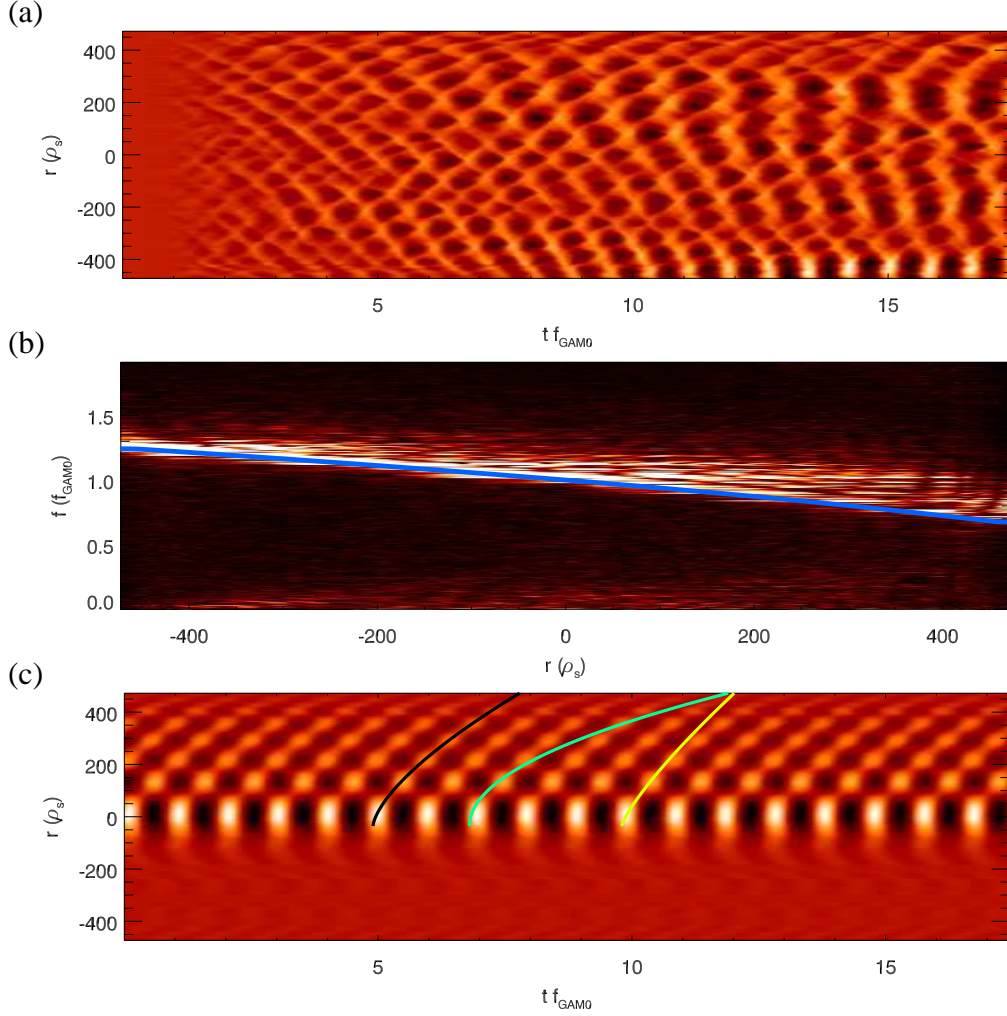
(a)

(b)

(c)

Figure 3: (a) GAM poloidal flow velocity for linear density and temperature profile, $\eta_i = L_n/L_T = 2.4, \varepsilon_n = .05, \alpha_d = 0.5$ (for definitions see [7]). $f_{GAM,0}$ is the GAM frequency at $r = 0$. (b) Frequency spectrum versus radius up to $tf_0 = 157$; linear GAM frequency (blue line). Note the GAM activity at $x = 300\rho_s$ at 140% of the linear frequency. (c) Filtered component at $f = 1.02f_{GAM,0}$; fit with $r(t) = c(t - t_0)^{2/3}$ (black), $r \propto (t - t_0)^{1/2}$ (green), $r \propto (t - t_0)^{4/5}$ (yellow).

α is much larger than expected from the linear dispersion.) Since the frequency is fixed in Fig. 3 (b), one obtains from a WKB argument

$$k_r = \sqrt{\left(\frac{\omega_{GAM}}{\gamma c_s(r)} - 1\right)/\alpha} \approx \sqrt{\frac{\partial_r \omega_{GAM}}{\alpha \omega_{GAM}(r_0,0)}(r_0 - r)}, \qquad (2)$$

with cut-off/reflection occuring at r_0 with $\omega_{GAM,0} = \gamma c_s(r_0)$. Any curve $r(t)$ of constant phase has to follow the equation

$$r'\partial_r\phi = \partial_t\phi \Rightarrow r'k_r(r) = \omega_{GAM} \Rightarrow r'\sqrt{(\partial_r\omega_{GAM}/(\alpha\omega_{GAM,0}))(r_0 - r)} = \omega_{GAM} \qquad (3)$$

$$\Rightarrow \frac{2}{3}\sqrt{-\partial_r\omega_{GAM}/(\alpha\omega_{GAM,0})}(r(t) - r_0)^{3/2} = \omega_{GAM}(t - t_0) \qquad (4)$$

$$\Longleftrightarrow r(t) = r_0 + \left[-\frac{9\alpha\omega_{GAM}^3(t - t_0)^2}{4\partial_r\omega_{GAM}}\right]^{1/3}. \qquad (5)$$
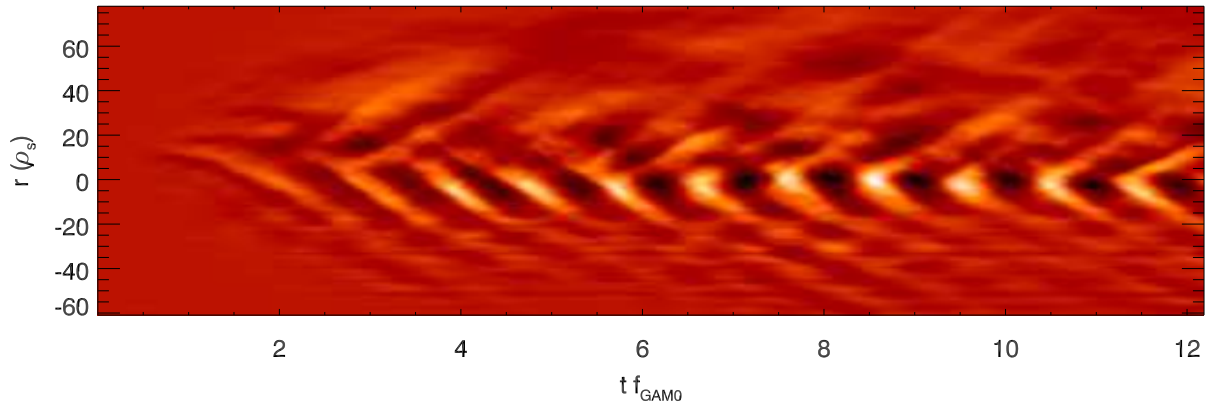
Figure 4: GAM poloidal flow for strong parameter variation. Parameters at center $\lambda = 50, \eta_i = 2.5, \varepsilon_n = 0.3$ (for details see [7] fig. 1b).

The predicted curve of form $r(t) = r_0 + c(t - t_0)^{2/3}$ has been fitted to one of the wave fronts in (c). A slightly different exponent results already in a misfit, corroborating the correctness of the ansatz (1) for the nonlinear dispersion relation. The dispersion coefficient $\alpha \approx 100\rho_s^2$ extracted from the fit is much larger than expected from linear GAM dispersion relations ($\sim \rho_s^2$) – it is thus a predominantly nonlinear effect. (The sign of α depends on the turbulence parameters. E.g., for higher $\eta_i \sim 5$ and otherwise identical parameters, the reflection scenario of the GAMs turns out to be exactly reversed.) The corresponding *nonlinear* group velocity [11] of the GAMs selected by the turbulence of order $\sim 10\rho_s\omega_{GAM}$ is even significantly larger than the maximum curvature drift velocities $v_d \sim \rho_s c_s / R$ which limit the linear group velocity of the GAMs [9, 10]. In other words, the GAM frequency in the presence of turbulence differs from the linear GAM frequency by a factor $1 + \alpha k_r^2$ ($\sim 30\%$ here), whereby, owing to the observed reflection layers, the actual k_r will depend also on the radial profile of the sound speed.

For sufficiently strong parameter variation, the GAMs may be generated only in a part of the computational domain, as shown in Fig. 4 for $\lambda = 50$. The GAMs radiate outward from the generation region at $r \sim 0$, maintaining their frequency, which indicates a radial energy transfer. The short radial decay length prohibits the straighforward application of the WKB method. The phase velocity is nevertheless directed outward from the point where the GAMs are generated, i.e., in the direction of the energy flow. The fact that phase velocity and energy flow point in the same direction is again consistent with (1) for positive α. In contrast to the case of weak parameter variation in the preceding section, the GAMs are damped by the turbulence away from the generation region and can therefore not propagate significant distances.

4. Summary

Numerical turbulence studies pertaining to edge paramters show that turbulence driven GAMs can control the transport – reducing it by a an order of magnitude – in situations where either strong diamagnetic effects give rise to the diamagnetic GAM drive due to fluctuating background profiles, or the free energy of pressure fluctuations (and with it the Stringe-Winsor driven GAM fluctuations) is much larger than the turbulence kinetic energy, such as in the edge and potentially in transport barriers. Due to the rapid parameter variation in the edge GAM regime, its radial dispersion becomes important, whereby the turbulent effects completely dominate the linear dispersive effects and greatly increase the radial group velocities. In the case of an extended region of GAM generating turbulence, propagation of the GAMs rather far away from the point of their base frequency can be observed. In the opposite case only a weak propagation

into regions where GAMs are damped occurs.

References

[1] K. Hallatschek, Plasma Phys. Control. Fusion **49**, B137 (2007)

[2] P. H. Diamond, S.-I. Itoh, K. Itoh, T.S. Hahm, Plasma Phys. Control. Fusion **47**, R35 (2005)

[3] S.-I.Itoh, et al., Plasma Phys. Control. Fusion **49**, L7 (2007)

[4] K. Hallatschek, D. Biskamp, Phys. Rev. Lett. **86**, 1223 (2001)

[5] G. D. Conway, et al., Plasma Phys. Control. Fusion **50**, 055009 (2008)

[6] A. Fujisawa, et al., Nucl. Fusion **47**, S718 (2007)

[7] K. Hallatschek, et al., Phys. Plasmas **7**, 2554 (2000)

[8] R. L. Miller, et al., Phys. Plasmas **5**, 973 (1998)

[9] R. Hager, K. Hallatschek, Phys. Plasmas **16**, 072503 (2009)

[10] R. Hager, K. Hallatschek, Phys. Plasmas **17**, 032112 (2010)

[11] R. Hager, K. Hallatschek, Phys. Plasmas *submitted*